Contents lists available at ScienceDirect

Fuel Processing Technology

journal homepage: www.elsevier.com/locate/fuproc

Continuous caustic aqueous phase electrochemical reforming (CAPER) of ethanol for producing compressed hydrogen

Benjamin L. Kee [a], Martinus Dewa [a,b], Osman Akpolat [c], Patrick Littlewood [c], James P. Seaba [d], Su Ha [a,e,*]

[a] The Gene and Linda Voiland School of Chemical Engineering and Bioengineering, Washington State University, Pullman, WA 99164, USA
[b] School of Mechanical and Materials Engineering, Washington State University, Pullman, WA 99164, USA
[c] Gas Technology Institute, Des Plaines, IL, 60018, USA
[d] Phillips 66 Research Center, Highway 60 & 123, Bartlesville, OK 74003, USA
[e] Chemistry Department, Washington State University, Pullman, WA 99164, USA

ARTICLE INFO

Keywords:
Ethanol electrochemical reforming
Hydrogen production
Hydrogen compression
Process intensification

ABSTRACT

Caustic Aqueous Phase Electrochemical Reforming (CAPER) of ethanol produces pure compressed H_2 at lower voltages, temperatures, and energy requirements than conventional electrolysis, while capturing carbonaceous products. The CAPER flow reactor consists of stainless steel endplates, stainless steel current collectors, and a Teflon flow field. The electrodes are prepared using commercial palladium nanoparticles on carbon support for the anode and platinum nanoparticles on carbon support for the cathode. The catalyst metal loading was 1 mg cm^{-2} on a 10 cm^2 carbon cloth for both electrodes. Our CAPER reactor produces pure H_2 at 80 bar and 80 °C applying voltages at ≤0.5 V. The only gas-phase product detected was H_2 and any carbonaceous products were contained in the liquid phase. The H_2 was produced with 97 ± 4% faradaic efficiency. Operating at smaller electrode separation distances (4 mm) and 80 °C increased the current density. The highest lower heating value efficiency achieved was 28% at a flow rate of 0.05 mL min^{-1} and an applied voltage of 0.5 V. The compressed H_2 was produced at ≤20 kWh kg^{-1}, which is much lower than electrolysis systems that require upwards of 50 kWh kg^{-1}.

1. Introduction

Hydrogen is an attractive energy carrier that can be used for both power generation and storage [1–4]. Currently, steam-methane reforming is the dominant H_2 producing process, but requires multiple unit processes including downstream water-gas-shift reactors, pressure swing adsorbers, and gas compressors [5,6]. Additionally, fossil-fuel based production of H_2 is not renewable and produces pollutants such as CO and CO_2 [7]. Electrolysis electrochemically splits water to generate H_2 and O_2. Water electrolysis provides a decarbonized approach to produce H_2, but is hindered by high electrical costs [8,9]. Electrolyzers are limited in operating pressure due to the increased gas permeation of H_2 and O_2 across the membrane at high pressures, which can lead to hazardous mixtures [8]. Therefore, electrolyzers require downstream multistage compression to achieve high-pressure H_2 delivery. Water electrolyzers typically require membranes to isolate the gas-phase products and can improve current densities by achieving small electrode separation distance. However, membrane-less electrolyzers have also shown advantages in reducing capital costs and are not limited by the membrane operating conditions [10].

Ethanol (C_2H_5OH) can be used as a feedstock for H_2 production due to its high volumetric H_2 content, ease of handling/transportation, and can be renewably produced biologically [11,12]. Steam reforming of ethanol produces H_2, CO, CO_2, and CH_4 but typically requires high temperature (> 300 °C) over precious metal catalysts [12]. Recent studies have shown aqueous-phase reforming as an effective method to

Abbreviations: Ag/AgCl, Silver/Silver chloride; CAPER, Caustic aqueous phase electrochemical reforming; EtOH, Ethanol; F, Faraday constant; GC, Gas chromatograph; I, Current; LHV_k, Lower heating value of species k; M_{H_2}, Molecular weight of H_2; $\dot{m}_k$, Mass flow rate of species k; $\dot{n}_k$, Molar flow rate of species k; NMR, Nuclear magnetic resonance; p, Pressure; Pd/C, Palladium on carbon; T, Temperature; V, Voltage; $w_{compression}$, Gas compression work; $W_{electric}$, Electrical power; W_{pump}, Liquid pump work; η_F, Faradaic efficiency; η_{LHV}, Lower heating value efficiency; ρ, Density; $X_{C_2H_5OH}$, Ethanol conversion; Y_{H_2}, Hydrogen yield.

* Corresponding author.
E-mail address: suha@wsu.edu (S. Ha).

https://doi.org/10.1016/j.fuproc.2023.107751
Received 31 December 2022; Received in revised form 15 March 2023; Accepted 25 March 2023

produce H_2 including options for in-situ CO_2 removal [13–15]. Aqueous-phase reforming of ethanol occurs at lower temperatures (< 300 °C) and high pressure (65 bar), but produces CH_4, CO_2, alkanes, and liquid-phase species in addition to the desired H_2 product [16]. Electrochemical oxidation of ethanol has demonstrated potential to produce H_2 at low energy requirements and low temperatures by utilizing electrochemical reactions [17–19]. The ethanol electro-oxidation reaction has been primarily studied in the context of direct ethanol fuel cells [20,21]. However, recent works have investigated using ethanol to electrochemically produce H_2. For example, Chen et al. used Pd nanoparticles on titania nanotubes to oxidize ethanol and produce H_2, while demonstrating energy savings of 26.5 kWh kg^{-1}[18]. Ruiz-Lopez et al. demonstrated ethanol electro-oxidation to produce H_2 on Pd/C and Pt/C in a membrane-less system, achieving 450 mA cm^{-2} at 1.4 V [17]. However, practical applications such as H_2 vehicle fueling stations require delivery of compressed H_2 [22–24]. Gas-phase compressors can contribute a significant cost in H_2 production [25]. The Caustic Aqueous Phase Electrochemical Reforming (CAPER) of ethanol delivers pure and compressed H_2 gas at low operating temperatures while circumventing inefficient gas-phase compression and downstream separation [26].

Fig. 1 illustrates the CAPER of ethanol process, which is an electrochemical process that produces pure H_2 at 80 bar pressure from ethanol solution while capturing carbon as an aqueous-phase carbonate. The liquid-phase reactants (i.e., ethanol and an alkaline electrolyte) are pumped into the electrochemical reactor by a liquid pump. Within the electrochemical flow reactor, H_2 and liquid-phase carbonates are produced. The gaseous H_2 easily separates from the liquid products in a knockout tank. The electrolyte can be regenerated by releasing a pure CO_2 stream via thermochemical [27] or electrochemical [28] methods.

The CAPER process provides several advantages over traditional processes. Compared to traditional methane steam reforming processes, CAPER does not require high temperatures, pressure swing adsorption, or gas compressors. Furthermore, the CAPER process provides fast kinetics for ethanol oxidation at a lower temperature range than conventional ethanol steam reforming (e.g., <200 °C) because it utilizes the electrical energy to facilitate the reaction. For example, the activation energy over the Pd anode for the electrochemical oxidation of ethanol in the CAPER process is reported as 16–35 kJ mol^{-1} [26], while the activation energy over the Pd catalyst for the ethanol steam reforming is in the range of 80–145 kJ mol^{-1} [29–31]. Even though these two reactions scenarios follow quite different reaction mechanisms, their comparison can present a basis for the range of activation energies, and highlights how electrochemical reactions are less dependent on temperature than thermally driven catalytic reactions. Moreover, the CAPER process can operate below 0.5 V, which significantly reduces the electrical energy requirement compared to the conventioal water electrolyzaer, does not need a membrane to separate the anode from the cathode, and performs liquid-phase compression instead of gas-phase compression [17,26]. The novelty of this work demonstrates a continuous flow reactor to produce 80 bar and pure H_2 at 97% ± 4% faradaic efficiency from ethanol electro-oxidation without downstream compression or gas-phase separation, while capturing carbonaceous products in the liquid phase.

2. Thermodynamics

On the anode, ethanol is oxidized in the presence of hydroxides (OH^-) to form CO_2 and H_2O. On the cathode, H_2O is reduced to form gaseous high-pressure H_2:

$$\text{Anode}: C_2H_5OH + 12\ OH^- \rightarrow 2CO_2 + 9H_2O + 12e^- \quad (1)$$

$$\text{Cathode}: 12H_2O + 12e^- \rightarrow 6H_2 + 12\ OH^- \quad (2)$$

The anodic and cathodic electrochemical reactions combine to arrive at the observed ethanol steam reforming reaction (Eq. (3)), where 6 moles of H_2 are produced for every mole of ethanol and 3 moles of H_2O reacted:

$$\text{Overall Reaction}: C_2H_5OH + 3H_2O \rightarrow 2CO_2 + 6H_2. \quad (3)$$

In alkaline conditions, the oxygen evolution reaction (OER) and ethanol reaction are written as:

$$O_2 + 2H_2O + 4e^- \leftrightarrow 4OH^- \qquad (E_0 = 0.401\ \text{V vs RHE}) \quad (4)$$

$$2CO_2 + 9H_2O + 12e^- \leftrightarrow C_2H_5OH + 12OH^- \qquad (E_0 = -0.744\ \text{V vs RHE}) \quad (5)$$

Thus, the OER is not a thermodynamically favorable reaction compared to the ethanol oxidation reaction. Furthermore, if OER is the dominant reaction, then the equilibrium cell potential should be approximately −1.23 V ($E_{cathode} - E_{anode} = -0.828\ V - 0.401\ V = -1.229\ V$). For our experiment, the operating cell potential of CAPER was only −0.5 V, which is much less than −1.23 V. Consequently, the

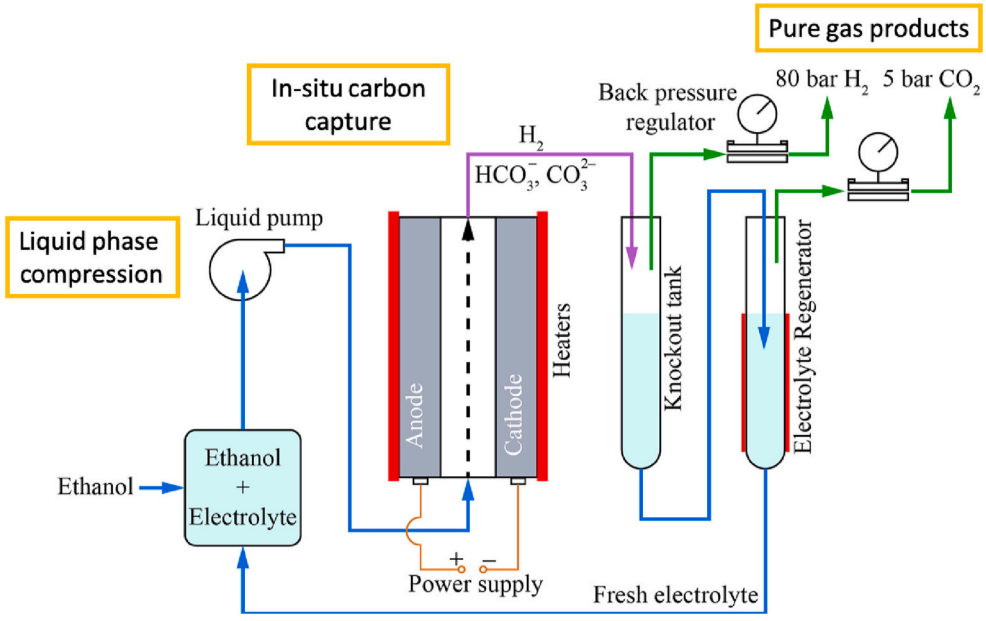

Fig. 1. Overview of a conceptual CAPER system, where ethanol is electrochemically oxidized on the anode and high-pressure hydrogen is produced on the cathode.

ethanol oxidation reaction on the anode does not compete with the OER in CAPER. At the cathode, CO_2 reduction is not favored. Even though the cell potentials for CO_2 reduction to CO and CH_3OH are thermodynamically possible at the cathode of CAPER (Table S1), the Pt catalyst at the cathode kinetically favors the H_2 evolution reaction in the aqueous phase with 95.7% faradaic efficiency [32].

There are electrical and thermal energy tradeoffs that are important in electrochemical H_2 production, where CAPER excels. Electrolysis can be divided into low-temperature and high-temperature regimes. The common low-temperature (50–80 °C) electrolyzer technologies are based on either polymer electrolyte membrane electrolyzers or alkaline electrolyte membrane electrolyzers [33]. On the other hand, the ceramic electrolyte membrane-based solid oxide electrolyzers operate at high temperatures (600–850 °C) [33–36]. All electrochemical cells require a minimum thermodynamic cell potential (ΔG) to produce H_2, also written as the Nernst potential. This thermodynamic cell potential decreases as the temperature increases, meaning high-temperature electrolyzers require lower operating voltages than low-temperature electrolyzers. The thermoneutral voltage (ΔH) separates the exothermic and endothermic operating regimes. Operating below the thermoneutral voltage and above the Nernst potential is the endothermic regime, where additional thermal heat is required. Above the thermoneutral voltage, the reaction is exothermic where cooling is required. The reversible heat demand ($T\Delta S$) increases with temperature.

Fig. 2 shows the voltage required and energy demand of water electrolysis and CAPER within their expected temperature ranges. The thermodynamic values were calculated from the global observed reactions, and the energy demand was calculated using 100% faradaic efficiency. In Fig. 2a) for the conventional water electrolysis, the temperature ranges from room temperature to 700 °C. Low-temperature electrolyzers generally require 1.23 V to split water. At 100 °C, where water boils, the voltage and energy demand drop due to the lower energy load of using steam versus liquid water. Solid oxide electrolyzer technologies advertise high-temperature operation for reduced operating voltage and improved kinetics. If operating at the thermoneutral voltage, a low-temperature electrolyzer requires approximately 1.5 V and 40 kWh kg^{-1} whereas high-temperature electrolyzers require approximately 1.3 V and 34 kWh kg^{-1}. In practical applications, the operating voltage is above the thermoneutral voltage to achieve higher current densities [8,34]. At the high current densities, the H_2 production rates are higher but at the sacrifice of efficiency [37].

In CAPER, the operating voltages and the energy demand are much smaller than in water electrolyzers. In Fig. 2b), the Nernst potential begins at 0.084 V at room temperature and can decrease below 0.05 V above 100 °C. Unlike electrolyzers, CAPER operates at high pressure such that liquid reactants water and ethanol will not boil at 100 °C. The thermoneutral voltage of CAPER is near 0.3 V, which correlates to an energy demand below 9 kWh kg^{-1}. This energy demand of CAPER is approximately 5 times smaller than what is required for water electrolysis. CAPER can also be paired with low-grade waste heat sources to operate closer to the Nernst potential but in the endothermic regime.

3. Experimental

3.1. Catalyst and electrode preparation

The electrodes were prepared using commercial palladium nanoparticles on carbon support (Sigma-Aldrich 407,305) on the anode and platinum nanoparticles on carbon support (Sigma-Aldrich 738,549) on the cathode. The palladium catalyst on the anode demonstrated high exchange current density and good stability in the alkaline environment [26] and platinum is an effective H_2 evolution reaction catalyst. The catalyst metal loading was 1 mg cm^{-2} on a 10 cm^2 carbon cloth (ETEK B1A). Inks were prepared using the 33 mg of catalyst powder mixed with 2640 µL of isopropyl alcohol (99.9%, Sigma-Aldrich) and 660 µL of 5 wt % Nafion® solution (Sigma-Aldrich 274,704). The resulting ink was thoroughly mixed using an ultrasonicating tip for 5 min. The ink was dripped onto the carbon cloth support in 200 µL aliquots. Between each application, the volatile components were allowed to evaporate under a heat lamp, leaving only the attached catalyst behind.

3.2. Electrochemical flow reactor

Fig. 3a) shows an illustration of the electrochemical flow reactor. The reactor had three major components: endplates, current collectors, and a flow field. The endplates were 2.5 cm thick 316 stainless steel to maintain a hermetic seal at 80 bar and 80 °C. Each endplate had a labyrinth seal to reduce leak pathways and improve sealing to the flow field. The endplates were held in compression by 12 bolts on the perimeter and electrically isolated using nylon sleeve washers. The Teflon flow field that acted as the gasket seal was placed between two endplates. The Teflon flow field was electrically insulating, malleable enough to be a gasket, and could operate at temperatures up to 150 °C. The flow field had the matching labyrinth seal ridge to seal onto either endplate. The electrodes and current collectors also fit between the endplates as shown in Fig. 3a). The flow channel had ridges for a 3 mm thick 316 stainless steel current collector, such that the separation between the electrodes was 4 mm. On this ridge, the carbon paper or cloth

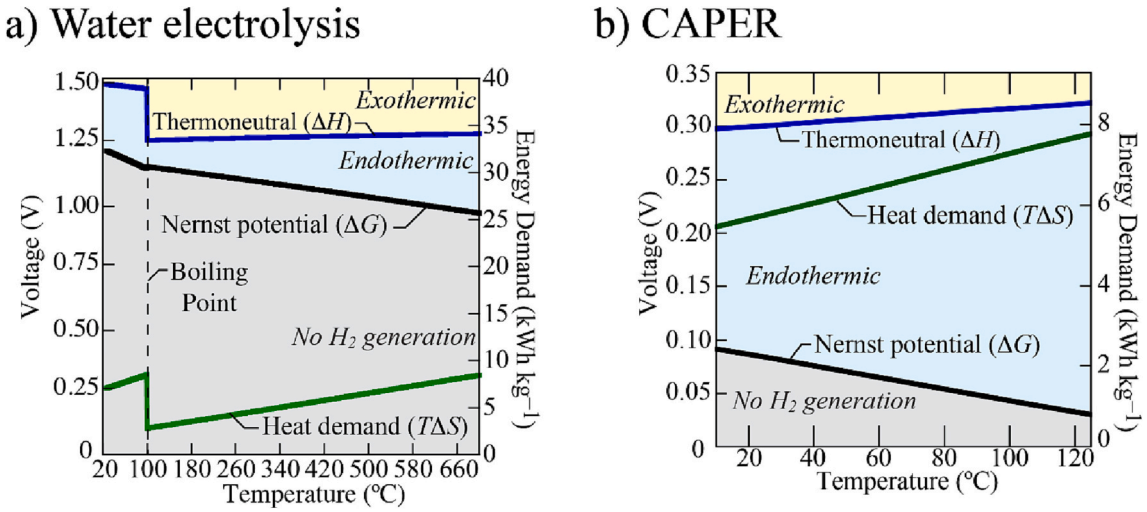

Fig. 2. Thermodynamic voltages and energy demand for a) Water electrolysis and b) CAPER.

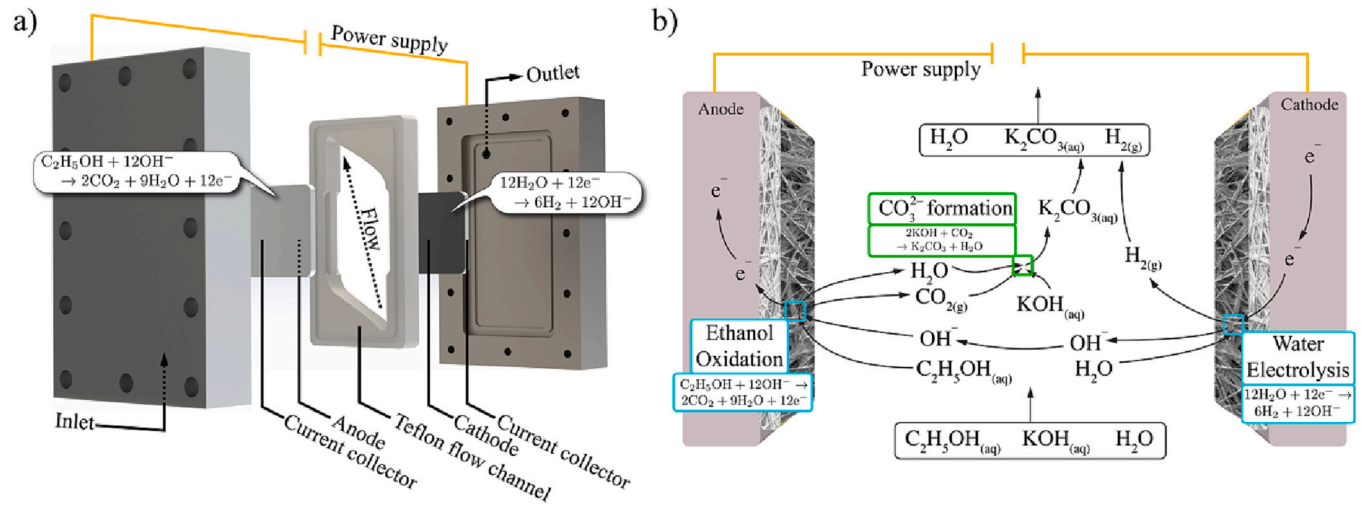

Fig. 3. a) Exploded view of planar flow reactor including end plates, current collectors, and electrodes and b) schematic describing the anodic and cathodic chemistries.

was pinned between the flow field and the current collector. Thus, the reaction volume was 100 mm × 100 mm × 4 mm.

The electrochemical flow reactor was operated at 80 bar. The pressure was achieved using a quaternary pump (Agilent 1100) for the liquid-phase reactants in conjunction with a biphasic back-pressure regulator (Equilibar) at the exit of the electrochemical flow reactor as shown in Fig. 1. The electrolyte concentration used was 4 M KOH, based on conductivity and catalyst activity in previous work [26]. The liquid and gas-phase products were separated in a knockout tank at atmospheric pressure. The gas-phase products were analyzed by gas chromatography (Agilent 490 Micro GC). A power supply (hp 6033A) set to the desired voltage provided power to the electrochemical flow cell and was attached to the electrical leads on the endplates. The heating of the reactor was achieved by cartridge heaters inserted into the endplates and heat tape leading into the reaction zone.

Fig. 3b) illustrates the chemical phenomena occurring inside the electrochemical reactor. The reactants ethanol, KOH, and H_2O flow into the reactor from the bottom using the liquid quaternary pump. The ethanol reacts on the anode to produce CO_2, H_2O, and e^-. On the cathode, H_2O and e^- are consumed to produce H_2. Any gas-phase CO_2 can be readily captured by aqueous KOH as aqueous K_2CO_3. The products exiting the reactor are aqueous K_2CO_3 and gaseous H_2.

3.3. Performance metrics

The performance of the electrochemical flow reactor was measured by conversion (X_{EtOH}), yield (Y_{H_2}), faradaic efficiency (η_F), and lower heating value efficiency (η_{LHV}) defined below:

$$X_{C_2H_5OH} = \frac{\dot{n}_{EtOH,in} - \dot{n}_{EtOH,out}}{\dot{n}_{EtOH,in}} \tag{6}$$

$$Y_{H_2} = \frac{\dot{n}_{H_2}}{6\dot{n}_{EtOH,in}} \tag{7}$$

$$\eta_F = \frac{2F\dot{n}_{H_2}}{I} \tag{8}$$

$$\eta_{LHV} = \frac{\dot{m}_{H_2}\left(LHV_{H_2} + w_{compression}\right)}{\dot{m}_{EtOH}LHV_{EtOH} + W_{pump} + W_{electric}}, \tag{9}$$

where $X_{C_2H_5OH}$ is the ethanol conversion, $\dot{n}$ is a molar flow rate, Y_{H_2} is the H_2 yield, η_F is the faradaic efficiency, F is the faraday constant, and I is the current. For calculating the LHV efficiency (η_{LHV}), LHV_k is the lower heating value of species k. The added value by delivering isothermally compressed H_2 is calculated as:

$$w_{compression} = \frac{RT}{M_{H_2}} ln\left(\frac{p_{outlet}}{p_{atm}}\right), \tag{10}$$

where R is the gas constant, T is the temperature, M_{H_2} is the molecular weight of H_2, p_{outlet} is the pressure of the delivered H_2, and p_{atm} is the atmospheric pressure. The liquid pump work is calculated as:

$$W_{pump} = (p_{outlet} - p_{atm})\frac{\dot{m}_{in}}{\rho_{in}}, \tag{11}$$

where $\dot{m}_{in}$ is the inlet mass flow rate and ρ_{in} is the density of the inlet stream. The electrical power supplied is calculated as:

$$W_{electric} = IV, \tag{12}$$

where I is the current and V is the applied voltage. The liquid concentrations were verified by proton NMR, and the gas concentrations were determined by gas chromatography. The liquid flow rate was measured by a graduated cylinder, and the gas flow rate was measured by the bubble flow meter. The H_2 production rate was calculated from the gas chromatograph measurement and the bubble flow meter measurement. Its detail calculation is explained in SI.

4. Results/Discussion

4.1. Product selectivity

H_2 purity is critical to downstream H_2 applications such as fuel cells. Common contaminants from reforming reactions such as CO can poison the catalyst of downstream processes. These contaminants require purification steps such as pressure-swing adsorption or membrane reactors. In CAPER, the carbon from the ethanol produces mostly gaseous CO_2 and some liquid-phase acetate ($C_2H_3O_2^-$). The total ethanol oxidation to CO_2 on the anode competes with the partial oxidation of ethanol to acetate [38,39] as the anode potential increases above −500 mV vs. Ag/AgCl [26]:

$$C_2H_5OH + 5OH^- \rightarrow C_2H_3O_2^- + 4H_2O + 4e^- \tag{13}$$

The $C_2H_3O_2^-$ is a liquid at the typical operating condition of CAPER system and does not dilute the gas-phase purity. However, the number of electrons per mole of ethanol reacted to produce $C_2H_3O_2^-$ is nearly half that of full oxidation to CO_2. Therefore, operating under conditions where CO_2 formation is favored, benefits the CAPER system for

achieving the high energy efficiency.

Carbon species were not detected in the gas phase because CO_2 was captured in the electrolyte. The 4 M KOH electrolyte is a strong base, that provides OH^- conductivity and can readily capture CO_2 as a liquid-phase carbonate (K_2CO_3) [40]:

$$2KOH + CO_2 \rightarrow K_2CO_3 + H_2O. \quad (14)$$

Potassium carbonates can be used in agriculture applications as a fertilizer [41,42]. Converting CO_2 into a liquid-phase carbonate eliminates the need for downstream purification because H_2 was the only gas-phase product. Additionally, CO production via the reverse water gas shift reaction was suppressed due to the low concentration of CO_2 [43]. When both CO_2 and H_2 exist, CO can be produced through the reverse water gas shift reaction. However, the CO_2 removal from the gas phase suppresses the reverse water gas shift reaction, and therefore no CO was formed. Additionally, any CO that may be produced could be oxidized on the anode [44]. CaO is an absorbant that has been used in aqueous phase reforming [45], but requires adding CaO to the solution, whereas the KOH electrolyte is already present in the system and KOH has been shown to be more cost effective [46].

Compared to other means of ethanol reforming, CAPER provides the highest H_2 gas purity. Table 1 shows the gas-phase compositions for CAPER, aqueous thermochemical reforming, and steam reforming processes. The major difference between these three processes is the operating temperature and pressure. The CAPER process offers the lowest operating temperature by utilizing the electrical energy to drive the reaction. In other words, the CAPER process provides the flexibility of using both the thermal and electrical energies in different proportions. Renewable energy sources can easily provide electrical energy input for the CAPER process. Aqueous thermochemical ethanol reforming requires pressures of 65 bar and temperatures near 250 °C. Ethanol steam reforming occurs above 300 °C and low pressure, such that ethanol and water are in the gas phase. The three cases considered here all use Pd supported on carbon catalyst. CAPER produces almost pure H_2 with at most 0.3 ppm of CO_2 at 80 bar. Aqueous thermochemical ethanol reforming and ethanol steam reforming both produce significant fractions of CH_4 and CO_2 in the gas phase. Consequently, these two processes both require an energy-intensive downstream separation process. On the other hand, the CAPER produces no CH_4, and the CO_2 produced becomes a liquid-phase carbonate. Table S2 shows a carbon balance on the CAPER reactor at voltages of 0.5 and 0.3. At both voltages, the inlet and outlet carbon was calculated to demonstrate carbon species balance within 1% error. Depending on the catalyst and operating conditions, the mole fractions of each process will vary, but CAPER is the only process that removes almost all of the CO_2 from the gas phase to produce a very pure H_2 product by converting the gas-phase CO_2 into the liquid-phase K_2CO_3.

Table 1
Gas-phase mole fractions of ethanol reforming reactions using CAPER, aqueous thermochemical reforming, and steam reforming processes using Pd supported on carbon catalyst.

		CAPER (this work)	Aqueous thermochemical reforming [16]	Steam reforming [47]
Conditions	Temperature (°C)	80	250	330
	Pressure (bar)	80	65	1
	Catalyst	Pd/C	Pd/C	Pd/C
Mole Fraction (%)	H_2	100	11	43
	CH_4	0	49	28
	CO	0	0	13
	CO_2	3e-5	29	16
	Alkanes	0	2.6	0

4.2. Faradaic efficiency

At the cathode, H_2 was produced from the alkaline H_2 evolution reaction written in Eq. (2). The faradaic efficiency (calculated using Eq. (8)) on the cathode quantifies what portion of the electrons contribute to H_2 production. Typical losses in faradaic efficiency include fuel/H_2 crossover, side reactions, leakage current, or solubility of H_2. In the CAPER process, fuel crossover was very low to non-existent because ethanol cannot electrochemically reduce at the cathode and does not interfere with the H_2 kinetics on the cathode [17]. Furthermore, H_2 gas produced at the cathode could not be easily oxidized at the anode due to the poor solubility of H_2 in concentrated KOH solutions [48] and low exchange current density for H_2 oxidation on Pd at high pH [49].

The faradaic efficiency was determined from the H_2 production rate and the current supplied. The H_2 production rate was measured by GC and bubble flow meter. The current was measured by the power supply at various voltages between 0 and 0.65 V. Fig. 4 shows the faradaic efficiency of the cathode in the electrochemical flow reactor. The biphase mixture at 80 bar was depressurized to atmospheric pressure at the back pressure regulator and a 1 L cylinder provided a buffer prior to flow rate and composition measurement. However, due to the large pressure difference and the nature of biphasic flow, there existed many fluctuations in the gas flow rate. The large fluctuations in flow rate can provide an observed faradaic efficiency over 100%, but when including the estimated error bars from measurements, the faradaic efficiency includes values below 100%. The average faradaic efficiency across the 16 reported measurements was calculated as $\eta_F = 97 \pm 4\%$. The high faradaic efficiency was also observed in similar membrane-less reactor studies for ethanol electro-oxidation [17,26]. This means that all the electrons produced by ethanol electro-oxidation were converted to H_2 on the cathode and all the produced H_2 exited the reactor.

4.3. Linear sweep voltammetry

Fig. 5 shows linear sweep voltammograms at the scan rate of 5 mV s^{-1} in 4 M KOH and 8% ethanol at 80 bar. In Fig. 5a), the temperatures were varied between 40 and 80 °C while using a 4 mm electrode separation. As temperature increased, the current density rose due to faster ethanol electro-oxidation kinetics and lower Nernst potentials.

The electrode separation in the electrochemical flow reactor was adjusted by removing the current collectors and attaching the electrodes directly to the endplate. The gap separation determines the ohmic drop across the alkaline electrolyte. The smallest gap achievable was desired to minimize the ohmic losses across the electrolyte. For this reason, many electrochemical devices use membranes that are on the order of μm thickness. The membrane also acts as a physical barrier preventing electrodes from shorting. In membrane-less systems, the separation distance is on the order of mm thickness. Small electrode gaps increase

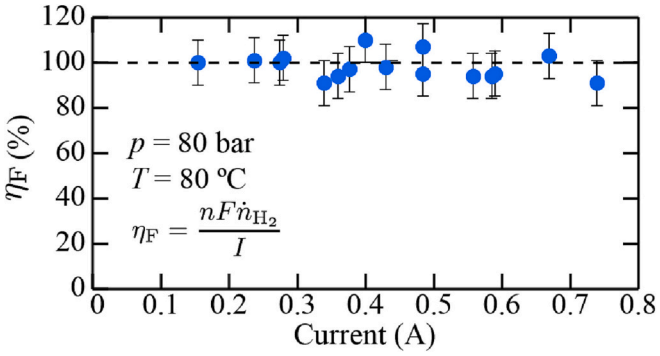

Fig. 4. Faradaic efficiency of H_2 production in the electrochemical flow reactor at measured currents between 0 and 0.8 A at 80 °C and 80 bar. Error bars are estimated from the fluctuations in gas flow rate at the biphase outlet.

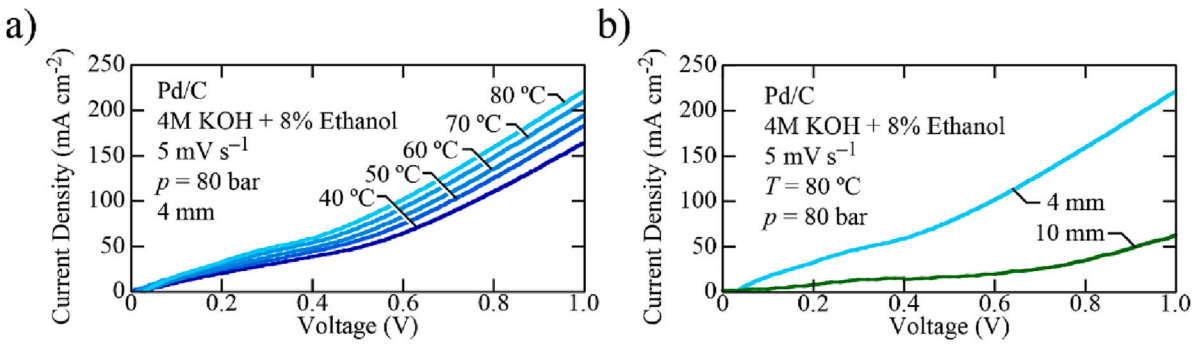

Fig. 5. Linear sweep voltammograms of a) temperatures between 40 and 80 °C and b) at electrode separation of 4 and 10 mm.

the likelihood of shorting when there is no physical separation. However, membrane-less systems can reduce capital costs and simplify reactor designs [10]. Fig. 5b) shows linear sweep voltammograms for a 4 mm gap and a 10 mm gap at 80 °C. At the thermoneutral voltage of 0.3 V, the 4 mm gap operates at 47 mA cm^{-2} whereas the 10 mm gap only operated at 13 mA cm^{-2}. Increasing the applied voltage or overpotential achieved higher current density, but selectivity toward unwanted side product acetate increased [26]. Therefore, operating near the thermoneutral voltage was advantageous for both product selectivity and energy efficiency.

4.4. Flow rate

Reducing the flow rate of reactants into the reactor increased the residence time, leading to higher conversion. The CAPER system benefited from high residence times, allowing more time for the ethanol to react over the catalyst. Fig. 6 shows the effect of flow rate on the ethanol conversion and the LHV efficiency of CAPER. The reactor volume was 100 mm × 100 mm × 4 mm. Thus, the range of liquid hourly space velocities for 0 to 2 mL min^{-1} is 0 to 3 h^{-1}. The values for the conversion and the LHV efficiency were closely linked. Based on Eq. (9), the LHV efficiency required high H_2 production rates to compensate for the LHV contributed by ethanol. Therefore, high conversion of ethanol into hydrogen was required to reach high LHV efficiencies.

In Fig. 6a), the conversion rapidly rose at low flow rates (0–0.5 mL min^{-1}), but at the highest flow rates (2 mL min^{-1}), the conversion was insignificant. The highest conversion achieved was 28%, which translated to a 28% LHV efficiency while operating at 0.5 V and 0.05 mL min^{-1} (liquid hourly space velocity of 0.075 h^{-1}). As the operating cell voltage increased from 0.3 V to 0.5 V, the conversion of ethanol increased for producing more hydrogen due to the increased kinetic activity. This increased ethanol conversion at the higher cell operating voltage led to higher LHV efficiency, despite larger electrical work. Even though CAPER was limited in ethanol conversion at these operating conditions, further improvement of the conversion will be achieved by improving current density via catalyst development with higher activity.

4.5. Ethanol concentration

Fig. 7 shows how varying the inlet ethanol concentrations affected the conversion, LHV efficiency, and current density of CAPER operating at two different flow rates. In Fig. 7a) and 7b), as the ethanol inlet concentration increased from 2 to 12%, the conversion and LHV efficiency decreased for both flow rates used, respectively. As the ethanol inlet concentration increased, the amount of ethanol that was fed to the reactor per unit time also increased. When this additional ethanol fed to the reactor did not convert (i.e., the low ethanol conversion and high ethanol inlet concentration condition), the LHV efficiency suffered as shown in Fig. 7b**)**. Hence, operating at low ethanol concentrations and low flow rates provided the highest LHV efficiencies, but at the expense of lower hydrogen production rates. Designing an anode catalyst that offers a higher kinetic activity toward full ethanol oxidation than Pd/C is needed for future improvements. Such a catalyst would allow operating the CAPER system at a high flow rate of ethanol to achive high hydrogen production rate while maintaining the high LHV efficiency.

For the reactor configuration shown in Fig. 3a), below 4% ethanol was when the current density started to decrease due to the transport limitations of ethanol. At dilute ethanol concentrations (<0.5 M), mass transfer limitations of ethanol to the anode lead to low current densities [17,50,51]. However, increasing the ethanol concentration to overcome mass transfer limitations also decreased the electrolyte ionic conductivity by decreasing the OH^- concentration, which reduced the current density [17]. This tradeoff in mass transfer and ionic conductivity caused the plateau in the current density as the ethanol concentration increased as shown in Fig. 7c**)**.

4.6. Energetic comparison

Fig. 8 shows a comparison of the energy required to produce 80 bar H_2 using either water electrolysis or CAPER. This comparison focuses on

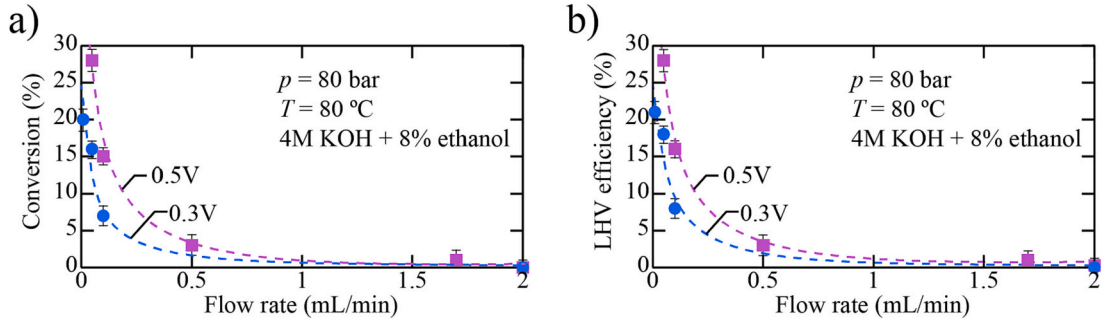

Fig. 6. The effect of flow rate on a) ethanol conversion and b) LHV efficiency at 80 bar, 80 °C, using 4 M KOH with 8% ethanol solution, and voltages of 0.3 and 0.5 V. Error bars are from repeated measurements. H_2 yield as a function of flow rate is shown in Fig. S1.

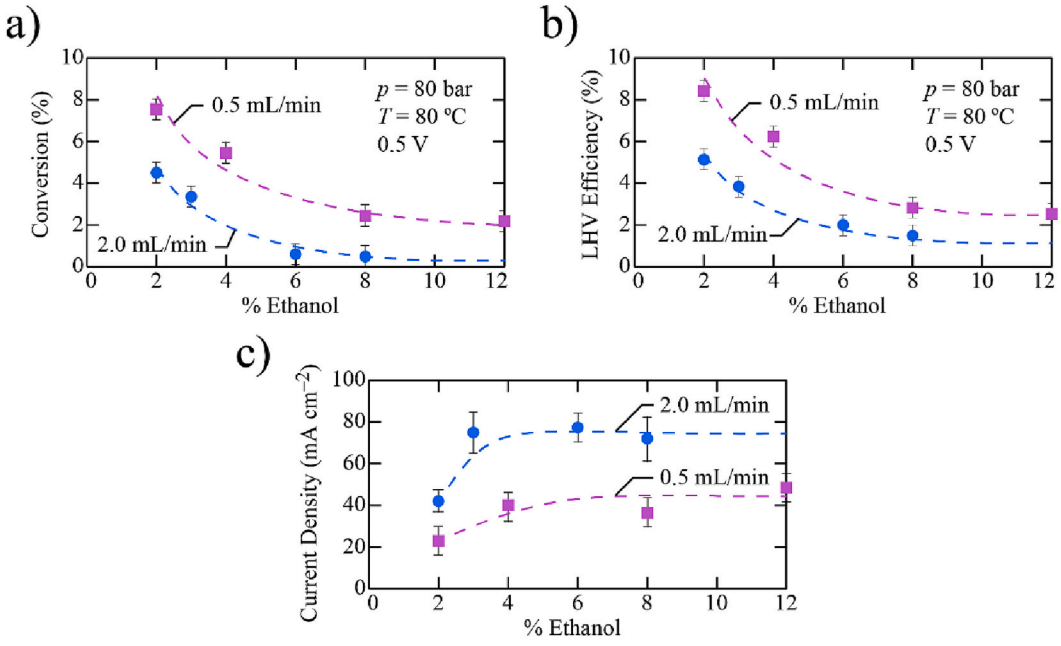

Fig. 7. The effect of ethanol concentration on a) ethanol conversion, b) LHV efficiency, and c) current density at 80 bar, 80 °C, 0.5 V and flow rates of 0.5 and 2.0 mL min^{-1}. Error bars are from repeated measurements. H_2 yield as a function of ethanol concentration is shown in Fig. S2.

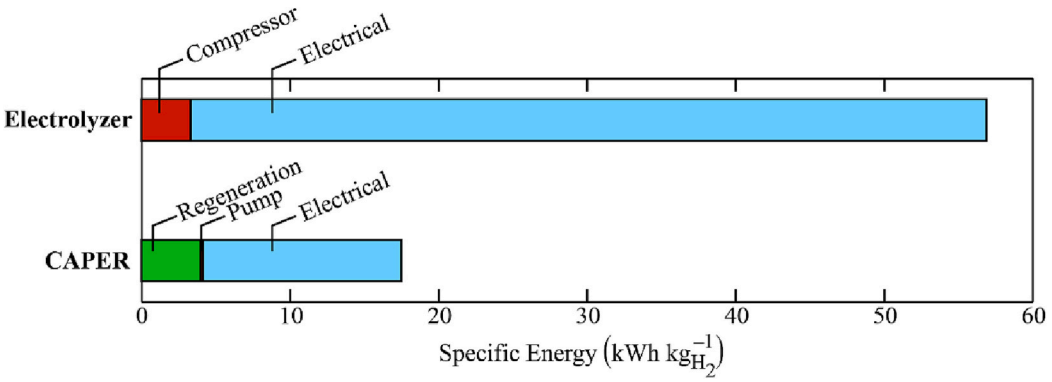

Fig. 8. Energetic comparison between a conventional electrolyzer and CAPER in units of kWh kg^{-1} of H_2 for 80 bar delivery.

the compression work and electrical work but does not include the balance of plant components, such as heating loads. The operating temperatures for both processes are similar and qualify as waste-grade heat. CAPER cannot yet achieve the same current densities as water electrolyzers and its operating cell voltage is >1 V lower than that of water electrolyzers. Therefore, the comparison occurs at 0.5 V over the thermoneutral voltage and is normalized by H_2 production rate. This allows both technologies to be compared at the same applied potential above the thermoneutral voltage to account for differences in cell voltages, and to normalize by the H_2 production rate to account for differences in current densities.

H_2 production using conventional low-temperature water electrolyzers generally requires 50–65 kWh kg^{-1} electrical energy and operates at 60% LHV efficiency [35]. The U.S. DOE H_2 demonstration refueling sites have reported an average compressor operation energy of 3.32 kWh kg^{-1} but can range from 0.5 to 10 kWh kg^{-1} and the average electrolyzer energy was 62.2 kWh kg^{-1} [52]. Many electrolyzers operate near 2.0 V to achieve high current densities [37], which is at least 0.5 V over the thermoneutral voltage. The 53.6 kWh kg^{-1} electrical work calculated here uses a 2.0 V operating voltage, and the compression work uses 3.32 kWh kg^{-1}.

For CAPER, the compression was achieved by a liquid-phase pump, which was calculated by Eq. (11). Liquid pump work is typically lower and less expensive than gas compressors due to the incompressibility of liquids versus the compressibility of gases. CAPER requires an additional electrolyte regeneration step to recycle the electrolyte as shown in Fig. 1. Electrochemical regeneration would require approximately 4 kWh kg^{-1} of H_2 [28]. The electrical work requirement for CAPER operating at 0.5 V is 13.4 kWh kg^{-1}. This study does not consider any work to generate the ethanol feedstock, which could have a significant impact on a life cycle analysis of the CAPER system.

In both processes, electricity was the dominating energy cost. However, CAPER requires much lower operating voltage, which significantly reduces the electrical power required. Electrolyzers require over 50 kWh kg^{-1} to produce compressed hydrogen, whereas CAPER can operate at <20 kWh kg^{-1}. In comparison to current practices, steam-methane reforming approximately costs 46 kWh kg^{-1} and is 72% efficient [6]. Between the major H_2 producing technologies, CAPER operates at the lowest kWh kg^{-1}.

5. Conclusions

CAPER of ethanol presents a process to produce pure and compressed H_2 at low voltages, low temperatures, and low energy requirements,

while capturing the carbonaceous products in the liquid phase. H_2 was produced at 80 bar and 80 °C while polarizing at 0.5 V and at 97 ± 4% faradaic efficiency. Higher H_2 production rates were achieved by operating at high temperatures (80 °C) and smaller electrode separation distances (4 mm). The highest LHV efficiency was 28% while using a flow rate of 0.05 mL min^{-1} and polarization of 0.5 V. The CAPER process produces compressed H_2 at <20 kWh kg^{-1}, which is significantly lower than electrolysis systems that require upwards of 50 kWh kg^{-1}. CAPER can be easily scaled up to operate at pressures above 80 bar because all the reactants remain in liquid phase.

This study demonstrates the CAPER process to produce compressed H_2. The process was limited by ethanol conversion, which leads to low LHV efficiencies. Future development of this process will require improved catalysts with higher exchange current densities and higher anode selectivity to CO_2. The present study only investigates the reactor in a single pass configuration, however stacking and recycling will further improve the conversion and efficiency. Despite the relatively low LHV efficiency, CAPER operates at significantly lower kWh kg^{-1} than water electrolyzers. Future development of this process will require improved catalysts with higher exchange current densities and lower noble-metal loading. Future work will also focus on the technoeconomic feasibility of the technology.

CRediT authorship contribution statement

Benjamin L. Kee: Methodology, Validation, Formal analysis, Investigation, Writing – original draft, Writing – review & editing, Visualization. **Martinus Dewa:** Validation, Formal analysis, Investigation. **Osman Akpolat:** Writing – review & editing, Supervision, Project administration. **Patrick Littlewood:** Writing – review & editing, Supervision. **James P. Seaba:** Conceptualization. **Su Ha:** Conceptualization, Methodology, Resources, Writing – review & editing, Supervision, Project administration.

Declaration of Competing Interest

The authors declare the following financial interests/personal relationships which may be considered as potential competing interests:

Su Ha reports financial support was provided by The RAPID Manufacturing Institute, USA. Su Ha reports financial support and equipment, drugs, or supplies were provided by Gas Technology Institute. Osman Akpolat reports a relationship with US Department of Energy that includes: funding grants. James P. Seaba reports a relationship with US Department of Energy that includes: funding grants.

Data availability

The authors do not have permission to share data.

Acknowledgments

This material is based upon work supported by the RAPID Manufacturing Institute, USA; the U.S. Department of Energy's Office of Energy Efficiency and Renewable Energy (EERE) under the Advanced Manufacturing Office Award Number DE-EE0007888; and GTI, USA under Project Number 22711. The authors acknowledge financial support from the O.H. Reaugh Laboratory at Washington State University for using its facility to perform reaction activity tests.

Appendix A. Supplementary data

Supplementary data to this article can be found online at https://doi.org/10.1016/j.fuproc.2023.107751.

References

[1] P.P. Edwards, V.L. Kuznetsov, W.I.F. David, N.P. Brandon, Hydrogen and fuel cells: towards a sustainable energy future, Energy Policy 36 (2008) 4356–4362.
[2] F. Dawood, M. Anda, G.M. Shafiullah, Hydrogen production for energy: an overview, Int. J. Hydrog. Energy 45 (2020) 3847–3869.
[3] J.O. Abe, A.P.I. Popoola, E. Ajenifuja, O.M. Popoola, Hydrogen energy, economy and storage: Review and recommendation, Int. J. Hydrog. Energy 44 (2019) 15072–15086.
[4] M. Yue, H. Lambert, E. Pahon, R. Roche, S. Jemei, D. Hissel, Hydrogen energy systems: a critical review of technologies, applications, trends and challenges, Renew. Sust. Energ. Rev. 146 (2021).
[5] T.S. Veras, T.S. Mozer, D.C.R.M. Santos, A.S. Cesar, Hydrogen: trends, production and characterization of the main process worldwide, Int. J. Hydrog. Energy 42 (2017) 2018–2033.
[6] I. Staffell, D. Scamman, A.V. Abad, P. Balcombe, P.E. Dodds, P. Ekins, N. Shah, K. R. Ward, The role of hydrogen and fuel cell in the global energy system, Energ, Environ. Sci. 12 (2019) 463–491.
[7] M. Momirlan, T.N. Veziroglu, Current status of hydrogen energy, Renew. Sust. Energ. Rev. 6 (2002) 141–179.
[8] M. Carmo, D.L. Fritz, J. Mergel, D. Stolten, A comprehensive review on PEM water electrolysis, Int. J. Hydrog. Energy 38 (2013) 4901–4934.
[9] P. Millet, S. Grigoriev, Water electrolysis technologies, in: P.M.D.L.M. Gandía, G. Arzamendi (Eds.), Renew. Hydrog. Technol. Prod. Purification, Storage, Appl. Saf., Elsevier, Amsterdam, 2013, pp. 19–41.
[10] D.V. Esposito, Membraneless electrolyzers for low-cost hydrogen production in a renewable energy future, Joule. 1 (2017) 651–658.
[11] S. Nanda, R. Rana, Y. Zheng, J.A. Kozinski, A.K. Dalai, Insights on pathways for hydrogen generation from ethanol, Sustain, Energy Fuel 1 (2017) 1232–1245.
[12] Y. Ma, X.R. Wang, T. Li, J. Zhang, J. Gao, Z.Y. Sun, Hydrogen and ethanol: production, storage, and transportation, Int. J. Hydrog. Energy 46 (2021) 27330–27348.
[13] G. Pipitone, G. Zoppi, R. Pirone, S. Bensaid, A critical review on catalyst design for aqueous phase reforming, Int. J. Hydrog. Energy 47 (2022) 151–180.
[14] P.D. Vaidya, J.A. Lopez-Sanchez, Review of hydrogen production by catalytic aqueous-phase reforming, ChemistrySelect. 2 (2017) 6563–6576.
[15] D. Liu, B. Dou, H. Zhang, K. Wu, C. Luo, J. Du, D. Xing Gao, H. Chen, Y. Xu, Sorption enhanced aqueous phase reforming of biodiesel byproduct glycerol for hydrogen production over Cu-Ni bimetallic catalysts supported on gelatinous MgO, J. Clean. Prod. 383 (2023), 135491.
[16] H. Xiong, A. DeLaRiva, Y. Wang, A.K. Datye, Low-temperature aqueous-phase reforming of ethanol on bimetallic PdZn catalysts, Catal, Sci. Technol. 5 (2015) 254–263.
[17] E. Ruiz-López, E. Amores, A. Raquel de la Osa, F. Dorado, A. de Lucas-Consuegra, Electrochemical reforming of ethanol in a membrane-less reactor configuration, Chem. Eng. J. 379 (2020), 122289.
[18] Y.X. Chen, A. Lavacchi, H.A. Miller, M. Bevilacqua, J. Filippi, M. Innocenti, A. Marchionni, W. Oberhauser, L. Wang, F. Vizza, Nanotechnology makes biomass electrolysis more energy efficient than water electrolysis, Nat. Commun. 5 (2014) 4036.
[19] A. Rodríguez-Gómez, F. Dorado, P. Sánchez, A.R. de la Osa, Boosting hydrogen and chemicals production through ethanol electro-reforming on Pt-transition metal anodes, J. Energy Chem. 70 (2022) 394–406.
[20] E.A. Monyoncho, T.K. Woo, E.A. Baranova, Ethanol electrooxidation reaction in alkaline media for direct ethanol fuel cells, Electrochem. 15 (2019) 1–57.
[21] M.Z.F. Kamarudin, S.K. Kamarudin, M.S. Masdar, W.R.W. Daud, Review: direct ethanol fuel cells, Int. J. Hydrog. Energy 38 (2013) 9438–9453.
[22] S. Satyapal, J. Petrovic, C. Read, G. Thomas, G. Ordaz, The U.S. Department of Energy's National Hydrogen Storage Project: Progress towards meeting hydrogen-powered vehicle requirements, Catal. Today 120 (2007) 246–256.
[23] U. Eberle, B. Müller, R. Von Helmolt, Fuel cell electric vehicles and hydrogen infrastructure: Status 2012, Energy Environ. Sci. 5 (2012) 8780–8798.
[24] B.L. Kee, D. Curran, H. Zhu, R.J. Braun, S.C. DeCaluwe, R.J. Kee, S. Ricote, Thermodynamic insights for electrochemical hydrogen compression with proton-conducting membranes, Membranes (Basel) 9 (2019).
[25] G. Sdanghi, G. Maranzana, A. Celzard, V. Fierro, Review of the current technologies and performances of hydrogen compression for stationary and automotive applications, Renew. Sust. Energ. Rev. 102 (2019) 150–170.
[26] B.L. Kee, W.-J. Wang, O. Akpolat, P. Littlewood, J.P. Seaba, L. Scudiero, S. Ha, Caustic aqueous phase electrochemical reforming (CAPER) of ethanol for process intensified compressed hydrogen production, Appl. Catal. A Gen. 641 (2022), 118647.
[27] M. Legarra, A. Blitz, Z. Czégény, M.J. Antal, Aqueous potassium bicarbonate/carbonate ionic equilibria at elevated pressures and temperatures, Ind. Eng. Chem. Res. 52 (2013) 13241–13251.
[28] F. Sabatino, M. Mehta, A. Grimm, M. Gazzani, F. Gallucci, G.J. Kramer, M. Van Sint Annaland, Evaluation of a direct air capture process combining wet scrubbing and bipolar membrane electrodialysis, Ind. Eng. Chem. Res. 59 (2020) 7007–7020.
[29] P.D. Vaidya, A.E. Rodrigues, Kinetics of steam reforming of ethanol over a Ru/Al2O3 catalyst, Ind. Eng. Chem. Res. 45 (2006) 6614–6618.
[30] D.R. Sahoo, S. Vajpai, S. Patel, K.K. Pant, Kinetic modeling of steam reforming of ethanol for the production of hydrogen over Co/Al2O3 catalyst, Chem. Eng. J. 125 (2007) 139–147.
[31] V. Mas, M.L. Bergamini, G. Baronetti, N. Amadeo, M. Laborde, A kinetic study of ethanol steam reforming using a nickel based catalyst, Top. Catal. 51 (2008) 39–48.

[32] A. Bagger, O. Christensen, V. Ivaništšev, J. Rossmeisl, Catalytic CO2/CO Reduction: Gas, Aqueous, and Aprotic Phases, ACS Catal. 12 (2022) 2561–2568.
[33] M. David, C. Ocampo-Martínez, R. Sánchez-Peña, Advances in alkaline water electrolyzers: a review, J. Energy Storage 23 (2019) 392–403.
[34] A. Hauch, R. Küngas, P. Blennow, A.B. Hansen, J.B. Hansen, B.V. Mathiesen, M. B. Mogensen, Recent advances in solid oxide cell technology for electrolysis, Science. 370 (2020).
[35] R. Hanke-Rauschenbach, B. Bensmann, P. Millet, Hydrogen production using high-pressure electrolyzers, in: V. Subramani, A. Basile, T. Nejat (Eds.), Compend. Hydrog. Energy, Woodhead Publishing, Cambridge, UK, 2015.
[36] R. Bhandari, C.A. Trudewind, P. Zapp, Life cycle assessment of hydrogen production via electrolysis - a review, J. Clean. Prod. 85 (2014) 151–163.
[37] F. Barbir, PEM electrolysis for production of hydrogen from renewable energy sources, Sol. Energy 78 (2005) 661–669.
[38] Y. Wang, S. Zou, W.-B. Cai, Recent advances on electro-oxidation of ethanol on Pt- and Pd-based catalysts: from reaction mechanisms to catalytic materials, Catalysts. 5 (2015) 1507–1534.
[39] L. Yaqoob, T. Noor, N. Iqbal, A comprehensive and critical review of the recent progress in electrocatalysts for the ethanol oxidation reaction, RSC Adv. 11 (2021) 16768–16804.
[40] E.S. Sanz-Pérez, C.R. Murdock, S.A. Didas, C.W. Jones, Direct capture of CO2 from ambient air, Chem. Rev. 116 (2016) 11840–11876.
[41] C.C. Mitchell, A.E. Hiltbold, N.V. Hue, Evaluation of a liquid potassium bicarbonate/amino acid co-product as a source of potassium, nitrogen, and sulfur, J. Plant Nutr. 17 (1994) 2119–2134.
[42] X. Han, X. Yan, X. Wang, J. Ran, C. Wu, X. Zhang, Preparation of chloride-free potash fertilizers by electrodialysis metathesis, Sep. Purif. Technol. 191 (2018) 144–152.
[43] K. Wu, B. Dou, H. Zhang, D. Liu, H. Chen, Y. Xu, Effect of impurities of CH3OH, CH3COOH, and KOH on aqueous phase reforming of glycerol over mesoporous Ni–Cu/CeO2 catalyst, J. Energy Inst. 99 (2021) 198–208.
[44] X. Cui, H.Y. Su, R. Chen, L. Yu, J. Dong, C. Ma, S. Wang, J. Li, F. Yang, J. Xiao, M. Zhang, D. Ma, D. Deng, D.H. Zhang, Z. Tian, X. Bao, Room-temperature electrochemical water–gas shift reaction for high purity hydrogen production, Nat. Commun. 10 (2019).
[45] K. Wu, B. Dou, H. Zhang, D. Liu, H. Chen, Y. Xu, Aqueous phase reforming of biodiesel byproduct glycerol over mesoporous Ni-Cu/CeO2 for renewable hydrogen production, Fuel. 308 (2022), 122014.
[46] A.A.H.I. Mourad, A.F. Mohammad, A.H. Al-Marzouqi, M.H. El-Naas, M.H. Al-Marzouqi, M. Altarawneh, CO2 capture and ions removal through reaction with potassium hydroxide in desalination reject brine: statistical optimization, Chem. Eng. Process. Process Intensif. 170 (2022), 108722.
[47] V.V. Galvita, V.D. Belyaev, V.A. Semikolenov, P. Tsiakaras, A. Frumin, V. A. Sobyanin, Ethanol decomposition over Pd-based catalyst in the presence of steam, React. Kinet. Catal. Lett. 762 (76) (2002) 343–351.
[48] P. Ruetschi, R.F. Amlie, Solubility of hydrogen in potassium hydroxide and sulfuric acid. salting-out and hydration, J. Phys. Chem. 70 (1996) 718–723.
[49] J. Zheng, W. Sheng, Z. Zhuang, B. Xu, Y. Yan, Universal dependence of hydrogen oxidation and evolution reaction activity of platinum-group metals on pH and hydrogen binding energy, Sci. Adv. 2 (2016).
[50] V. Alzate, K. Fatih, H. Wang, Effect of operating parameters and anode diffusion layer on the direct ethanol fuel cell performance, J. Power Sources 196 (2011) 10625–10631.
[51] A. Caravaca, A. De Lucas-Consuegra, A.B. Calcerrada, J. Lobato, J.L. Valverde, F. Dorado, From biomass to pure hydrogen: Electrochemical reforming of bio-ethanol in a PEM electrolyser, Appl. Catal. B Environ. 134–135 (2013) 302–309.
[52] S. Sprik, J. Kurtz, G. Saur, S. Onorato, M. Ruple, C. Ainscough, Next Generation Hydrogen Station Composite Data Products: All Stations (Retail and Non-Retail Combined), United States. https://www.nrel.gov/docs/fy18osti/71644.pdf, 2018.